Isothermal crystallization of isotactic polypropylene–hexamethylbenzene blends: crystal morphology

Ali A. Alwattari and Douglas R. Lloyd*
Department of Chemical Engineering, Center for Polymer Research, The University of Texas at Austin, Austin, TX 78712, USA
(Received 13 October 1993; revised 12 November 1993)

Lamellar crystal organization and spherulite formation were investigated as functions of melt polymer concentration and isothermal crystallization temperature for the model eutectic-forming system isotactic polypropylene (iPP) and hexamethylbenzene. Permanganic etching and scanning electron microscopy were used to reveal iPP crystal features. The results were interpreted in terms of the kinetics of crystallization events during thermally induced phase separation of this system.

(Keywords: isotactic polypropylene; hexamethylbenzene; crystal morphology)

INTRODUCTION

Microporous membranes can be formed by melt blending a semicrystalline polymer and a low-molecular-weight diluent, removing the thermal energy to induce phase separation and removing the diluent. Details of this thermally induced phase separation (TIPS) technique for membrane formation and the factors controlling the resulting structure have been reported[1–16]. During the solidification of melt blends of isotactic polypropylene (iPP) and various diluents by TIPS, the mobility, morphology and crystallization kinetics of the diluent have been shown to influence significantly solid structure development[4–10]. Of particular interest are the unique structures that can be formed when a crystallizable diluent, such as hexamethylbenzene (HMB), is used with iPP. Another paper in this series[17] demonstrates that the HMB often crystallizes prior to the onset of iPP crystallization or simultaneously with iPP crystallization. This paper reports the structure resulting from these two scenarios. Although many studies have been conducted on melt-crystallized iPP structure in pure and blended form[18–25], no previous systematic isothermal crystallization structure studies have been conducted on iPP blended with high-melting-temperature diluents. This study aims to elucidate the effect of the independent processing variables crystallization temperature (T_c), degree of supercooling (ΔT) and weight fraction iPP (W_p) on the lamellar and spherulitic morphological response of iPP to the presence of HMB during TIPS.

MATERIALS AND METHODS

Details regarding the materials and solid polymer–diluent sample preparation methodology are presented elsewhere[17]. Polymer concentrations of 30, 50, 70, 90 and 100 wt% were prepared.

Approximately 0.1 g of solid polymer–diluent blend was cut from the test-tube sample and placed in a small borosilicate glass vial (inside diameter = 8 mm, height = 35 mm, wall thickness = 1 mm). The tube was again purged, sealed and homogenized into a transparent melt at 500 K. Homogeneous samples were rapidly transferred to another oven, or quenched in a cold medium, preset to an isothermal temperature T_c between 273 and 423 K, and maintained until crystallization was complete[26]. The bulk of the sample plus the thickness of the borosilicate wall precluded sample crystallization during the 4–5 s transfer time. Thus, structure formation is assumed to be isothermal. The use of a relatively large sample prevented interference by surface effects or thermal strain, both of which may occur for thin samples. The upper T_c limit was determined by the equilibrium melting temperature at a particular polymer concentration[17].

Following the isothermal crystallization step, samples were quenched in an ice–water bath. Any atactic, lower-molecular-weight or incompletely crystallized isotactic polymer solidified during the quench possessed poorly crystallized or extremely small crystalline features[27]. Since these features would be less detectable than the dominant lamellae at a given magnification, they should not interfere with the analysis of isothermally formed structures[28].

To provide a uniform, reproducible surface for chemical etching and microscopy, one of the circular ends of the crystallized samples was cut at room temperature using a glass knife mounted in a Reichert–Jung Ultracut E microtome (C. Reichert Optische Werke). The cutting process was optimized in terms of temperature, cutting speed, knife angle and specimen size to minimize knife marks and other artifacts that prevent observation of the actual crystalline surface[29]. A vertical cutting speed of

* To whom correspondence should be addressed

0032-3861/94/13/2710–06

20 ± 2 mm s^{-1} and room conditions (293 ± 5 K) were used to cut the iPP samples. This procedure removed about 1 μm of surface during each vertical stroke against the glass knife. The surface was considered smooth when successive slices of blend were of consistent thickness, diameter and physical appearance. An additional requirement was that structures be representative of the bulk sample, free of interfacial effects during crystallization. Therefore, a depth of at least 500 μm was removed from the end of a sample.

Good reproducibility and agreement of pure iPP features (the control) with previous data[30] indicated successful cutting conditions had been achieved.

To implement scanning electron microscopy (SEM) it was necessary to expose the crystalline organization by solution etching. Without etching, there is insufficient contrast between polymer lamellae and surrounding material, such as amorphous polymer. The technique used in this study consists of selectively removing the less ordered material via a chemical reaction with a permanganic etchant[31]. This method has also been used successfully to reveal representative lamellar structures in melt-crystallized polyolefins[31–33] and in eutectic systems crystallized in a temperature gradient[34]. Gaseous ion etching has also successfully revealed polyolefin morphologies[35].

Prior to etching, samples were soaked in acetone to remove any HMB crystals in the vicinity of the surface to be examined. Extraction times of 72 h were used for all samples. Although in some cases these times are less than the time required for bulk diluent extraction, they were sufficient to allow reproducible observation of surface features. Failure to remove HMB resulted in its sublimation upon exposure to vacuum.

Etchant was prepared by slowly adding 0.7 wt% $KMnO_4$ to a 60:40 (by volume) mixture of H_2SO_4 (Sulfuric acid, 66° Baumé, UN1830 Technical Grade Fisher Scientific A-298, lot 744870) and dry H_3PO_4 (Phosphoric acid, 85%, UN1805 Fisher Scientific A-242, lot 865770). Mixing was performed at room temperature with rapid stirring (Corning Stirrer PC-353), yielding a fuming dark green oxidizing agent[36]. Approximately 10 ml of etching solution was poured into a small glass bottle containing the cut sample. The bottle was sealed with a ground-glass stopper to prevent air oxidation of the solution and placed in an ultrasonic bath (Branson model 2200). The etching time necessary to reveal clear features was found to be 5–6 h at room temperature. Finally, the sample was washed for 90 s with 2:7 (by volume) mixture of cold H_2SO_4/H_2O (≈ 253 K) to remove Mn and K from the etched surface[32], cleaned in hydrogen peroxide solution for 90 s to remove any sulfurous deposits from the surface, and rinsed in distilled water to remove residual hydrogen peroxide.

Prior to SEM observation, samples were coated with a gold–palladium film using a sputter coater (Commonwealth model 3, Pelco Catalog. No. 91000). A plasma current of 18 mA was used to generate the sputtering atoms from the gold–palladium target. A JEOL JSM 35C scanning electron microscope was used to examine the etched, extracted samples. A recommended accelerating voltage of 25 kV was used to accelerate the electron beam towards the sample surface. Two to three samples were prepared at each T_c, W_p combination to ensure that the photomicrographs represented typical features. Each sample was viewed at different locations before taking a picture, so that the features photomicrographed were typical rather than incidental.

RESULTS AND DISCUSSION

Structural trends are described as a function of W_p, T_c and ΔT (defined as the difference between the equilibrium melting temperature of iPP in the iPP–HMB blend[17] and T_c).

Pure iPP

There are four types of crystal structure for iPP reported in the literature: α or monoclinic[37], β or hexagonal[38,39], and two rare forms, γ (formed at high pressures) and δ (found in samples with high amorphous content). All four have the characteristic 3/1 helix, but are distinct in the way the helices are geometrically stacked. The α form is predominant at small ΔT ($T_c > 409$ K). The lamellar morphology of α is branched lamellae with a mixture of radial lath-like lamellae and tangential lamellae. The ratio of tangential to radial lamellae has been shown to decrease as T_c is increased. Moreover, at higher T_c, the radial lamellae were long and straight[21]. The β form is predominant at large ΔT ($T_c < 409$ K). The morphology is broad lamellae that are locally parallel and stacked with a sheaf-like overall geometry. The lamellae are extended sheets in all lateral directions[21].

Pure iPP structures were investigated in the T_c range 413 to 375 K ($\Delta T = 47$ to 85 K). *Figure 1* shows coarse, woven and splayed lamellar laths ≈ 0.1 μm thick at $\Delta T = 57$ K, typical of monoclinic structures associated with relatively small supercooling[21]. As ΔT was increased, lamellar coarseness decreased. *Figure 2* shows a sheaf-like sperulite formed at $\Delta T = 85$ K. Sheafing is characteristic of a hexagonal lattice contained in a β spherulite when $\Delta T > 54$ K[21]. The corresponding lamellae appear to be locally stacked and similar to those found in spherulites of other polymers[21].

90 wt% iPP

Lamellar features remained intact for 90 wt% samples crystallized in the T_c range 423 to 375 K ($\Delta T = 31$ to 79 K). In the range $\Delta T = 31$ to 61 K, all samples showed tightly woven, splayed, radial laths, indicative of monoclinic iPP crystal lattice (typified by *Figure 3*). As ΔT was

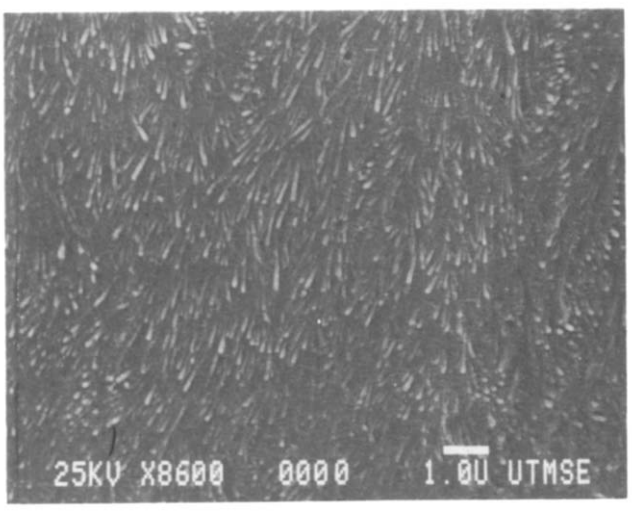

Figure 1 Tightly woven, splayed lamellar laths formed from pure iPP crystallized at $\Delta T = 57$ K ($T_c = 403$ K)

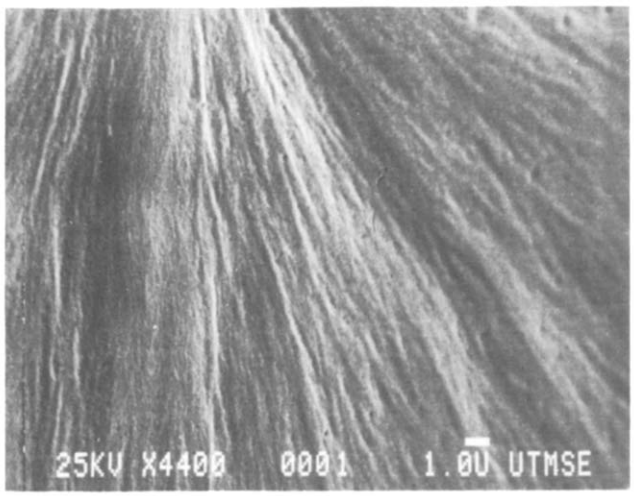

Figure 2 Sheaf structures emanating from a central region; formed from pure iPP crystallized at $\Delta T = 85$ K ($T_c = 375$ K)

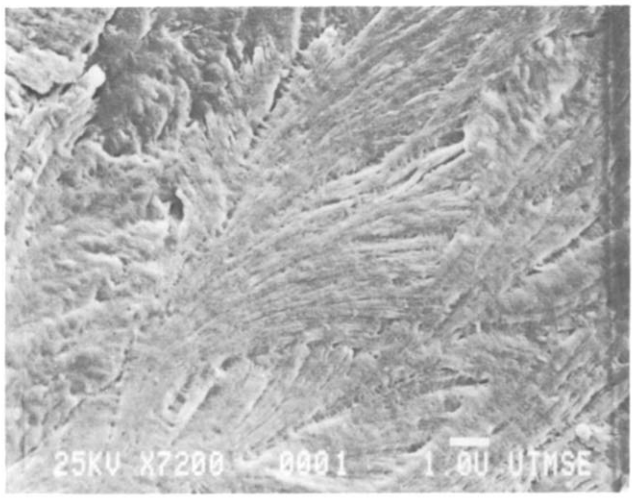

Figure 3 Coarse lamellar laths formed from 90 wt% iPP melt blend crystallized at $\Delta T = 51$ K ($T_c = 403$ K)

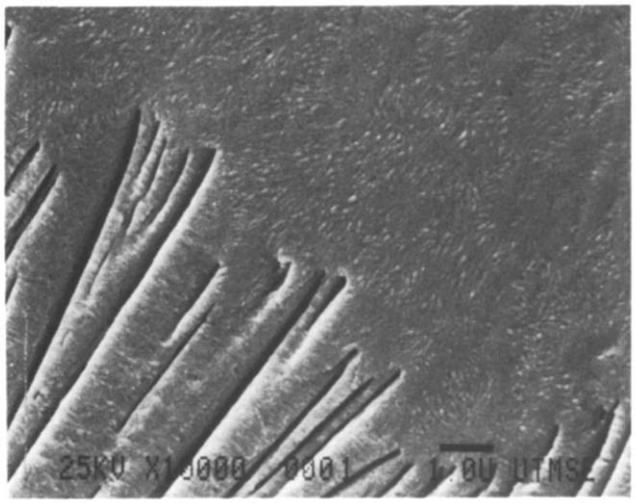

Figure 4 Details of lamellar ends adjacent to thin voids; formed from 90 wt% iPP melt blend crystallized at $\Delta T = 79$ K ($T_c = 375$ K)

increased, lamellar coarseness decreased. At $\Delta T = 79$ K, some details of lamellar ends and spherulite boundaries adjacent to thin pores were within the microscope resolution (*Figure 4*); however, lamellar details were not clearly resolved.

Spherulite diameter decreased as ΔT was increased; diameter sizes for $\Delta T = 31$, 51 and 79 K were 500, 200 and 60 μm, respectively. Also, as ΔT was increased, mutual spherulite impingement decreased because of spherulite size reduction and the formation of the porous interspherulitic microstructure. Spherulite size reduction is associated with increased heterogenous nucleation density as ΔT increases, and needle-like microstructure is associated with an increased fraction of iPP crystallizing in a eutectic mixture with HMB at lower T_c (ref. 17).

70 wt% iPP

As the polymer concentration was decreased to 70 wt%, the lamellar structure remained radial, splayed and lath-like in the supercooling range 29 to 49 K (*Figures 5* and *6*). As ΔT was increased, more cross-hatching was observed and lamellar coarseness decreased. Spherulite boundaries were slightly deformed in the vicinity of the pores, but were otherwise undisturbed. Studies on the relative kinetics of HMB and iPP suggested that HMB crystals should emerge prior to iPP crystallization under the T_c conditions used[17]. Therefore, the slight deformation of spherulites is corroborated. Spherulite diameter decreased from ≈ 100 to ≈ 30 μm as ΔT was increased

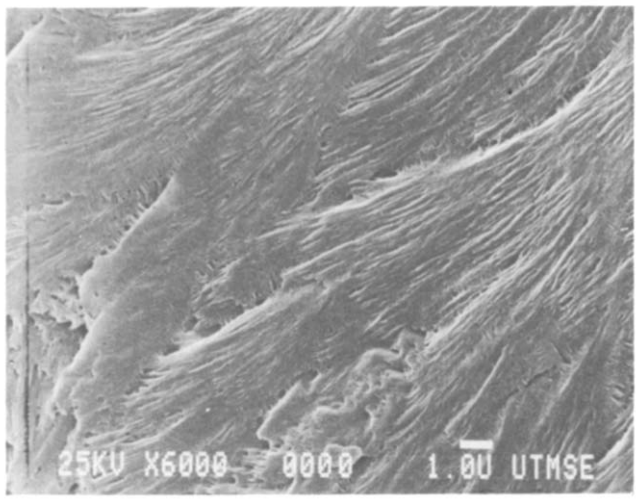

Figure 5 Splayed, cross-hatched lamellar laths formed from 70 wt% iPP melt blend crystallized at $\Delta T = 39$ K ($T_c = 403$ K)

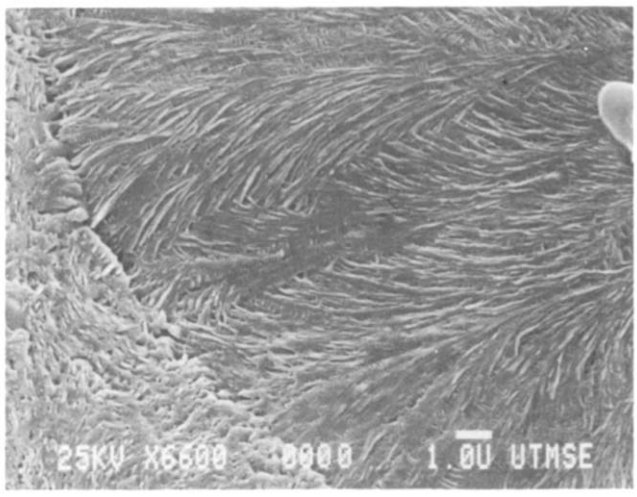

Figure 6 Splayed, cross-hatched lamellar laths formed from 70 wt% iPP melt blend crystallized at $\Delta T = 49$ K ($T_c = 393$ K)

from 29 to 49 K, while spherulites were not discernible for $\Delta T = 59$ to 169 K ($T_c = 273$ K). As ΔT is increased, increased nucleation density increases crystallization rate, reduces average spherulite size and increases the probability of inhibition of spherulite development by the mutual disruption of structure during rapid crystallization of iPP and HMB.

50 wt% iPP

At 50 wt% polymer concentration, lath-like lamellae were again the dominant morphology. As ΔT was increased from 18 to 38 K, the straightness of lamellae decreased, the frequency of tangential branches increased and the spherulite diameter decreased (*Figures 7* and *8*). Both figures show cross-hatching, which is typical of small supercoolings. The structure perfection indicates that iPP growth is undisturbed by HMB at the lamellar scale. Meanwhile, spherulite growth was deformed in the vicinity of needle-shaped pores, as clearly shown in *Figure 9*, which shows one such pore of radius $\approx 12\,\mu$m. The spherulite seems to have grown around or 'occluded' the HMB crystal from which the pore formed. Such deformation is a consequence of diluent separating from the melt prior to polymer crystallization, as demonstrated by relative kinetic studies of iPP–HMB[17]. Spherulites not adjacent to pores retained a perfect geometry (*Figure 7*).

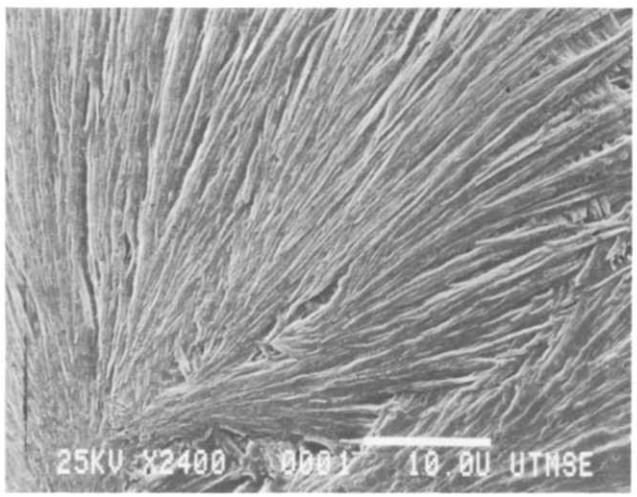

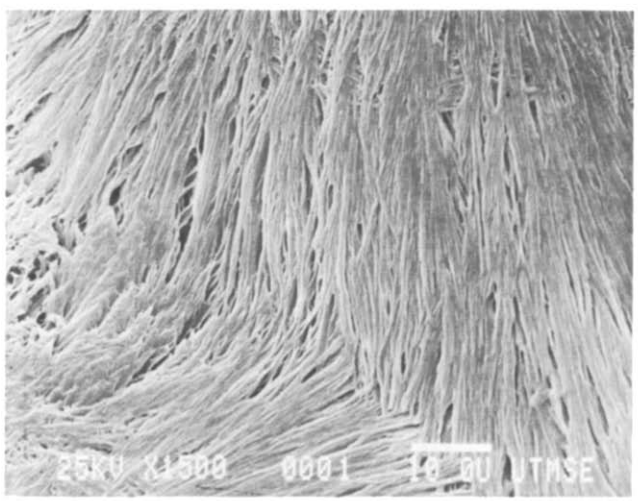

Figure 7 Straight, coarse lamellar laths formed from 50 wt% iPP melt blend crystallized at $\Delta T = 18$ K ($T_c = 413$ K). The lower figure shows intersection of two spherulites

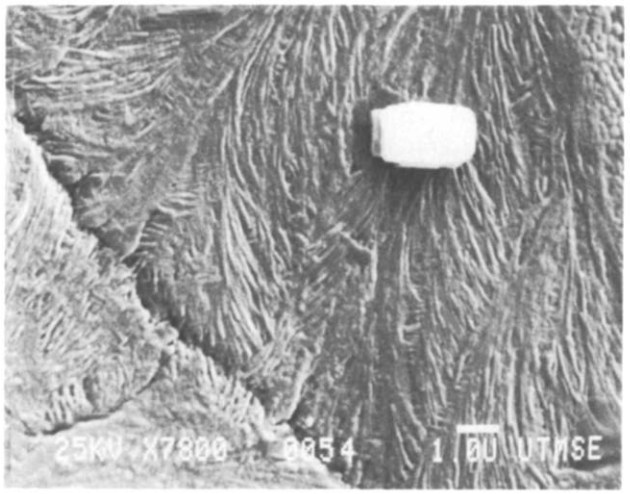

Figure 8 Lamellar laths at a spherulite boundary; formed from 50 wt% iPP melt blend crystallized at $\Delta T = 38$ K ($T_c = 393$ K)

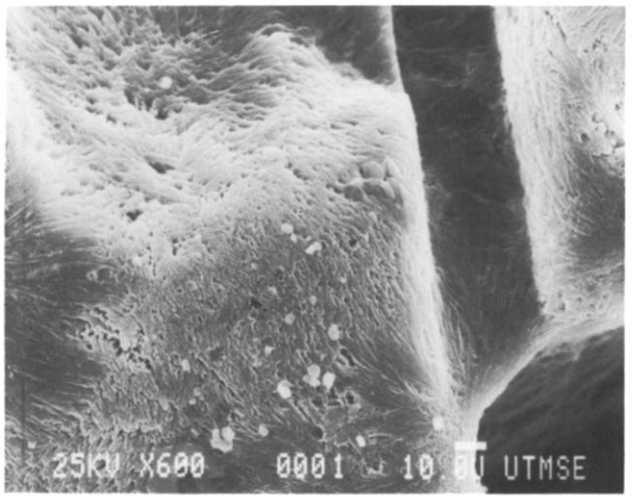

Figure 9 Spherulite structure near a pore formed by an HMB crystal (subsequently removed); 50 wt% iPP crystallized at $\Delta T = 18$ K ($T_c = 413$ K)

Occlusion of the HMB crystals by the crystallizing iPP is in agreement with published interfacial phenomena studies in crystallizing polymer blends[40], which suggest that more energy is required to displace large dispersed crystals in crystallizing polymer solutions than simply to grow around the crystals.

Spherulites were not discernible for $\Delta T > 56$ K; instead a needle-like microstructure, attributed to simultaneous crystallization of iPP and HMB, was observed (*Figure 10*). At a quench temperature of 273 K ($\Delta T = 158$ K), fibrillar polymeric structures crossing individual pores are observed (*Figure 11*). The mutual disruption of polymer and diluent crystal structures was probably caused by the extremely rapid crystallization rate of both components at the low temperature and large driving force. The nucleation density for both components rises sharply as supercooling is increased, according to classical nucleation theory. Meanwhile, the rapidly increasing medium viscosity reduces the mobility of diluent molecules. Thus, the probability is high for a diluent molecule to be immobilized at an adjacent nucleus prior to agglomeration into a non-adjacent growing crystal[8,9]. The reduced size scale of the HMB crystals is

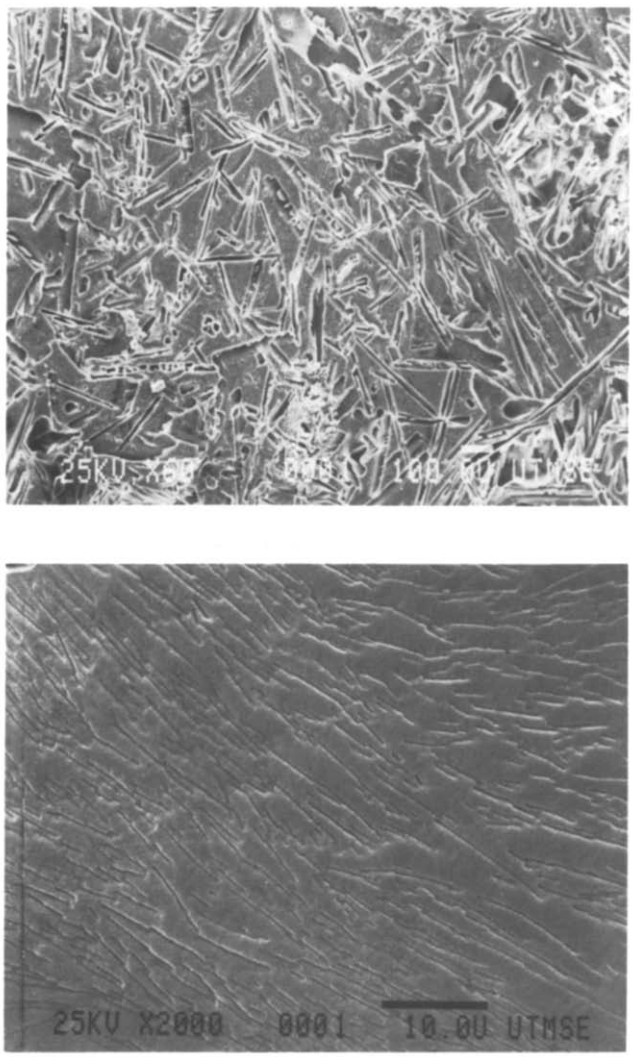

Figure 10 Primary and interspersed secondary needle-like pores; formed from 50 wt% iPP crystallized at $\Delta T = 56$ K ($T_c = 375$ K)

more likely to disrupt spherulite formation; hence, no discernible polymer superstructure develops.

30 wt% iPP

The lamellar structures formed at 30 wt% iPP were almost identical to those formed at 50 wt% in the same ΔT range of 18 to 38 K; the only difference was an increase in space between lamellar laths; that is, the polymer between large pores is more 'open' than in the samples formed from melt blends of higher polymer concentration (see *Figure 12*). As ΔT was increased, the straightness of lamellae, the visibility of cross-hatching and the coarseness of lamellae decreased. Lamellar lath or bundle size decreased from ≈ 0.6 to 0.1 μm as ΔT was increased from 18 to 38 K. Spherulite deformation by needle-shaped pores was again apparent, as shown in *Figure 12*. Spherulites were not discernible for $\Delta T > 56$ K (*Figure 13*) as in the case of 50 wt% polymer sample.

CONCLUSIONS

Lamellar features typical of pure iPP were manifested over the entire polymer concentration range investigated: 30 to 100 wt% polymer. Therefore, the presence of HMB did not prevent chain-folded lamellar crystal growth. This finding supports the applicability of a chain-folded mechanistic equation to describe growth rate[17]. However, at extremely low quench temperatures (large supercoolings), such as 273 K, mutually disrupted structures appeared on a size scale approaching that of lamellar bundles.

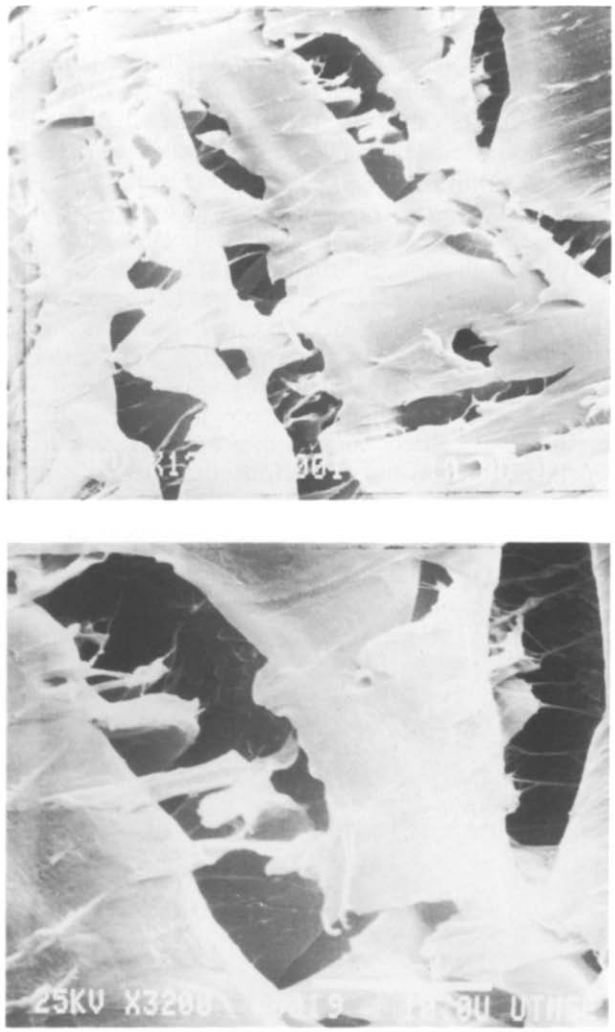

Figure 11 Two views of disrupted pores formed from 50 wt% iPP crystallized at $\Delta T = 158$ K ($T_c = 273$ K)

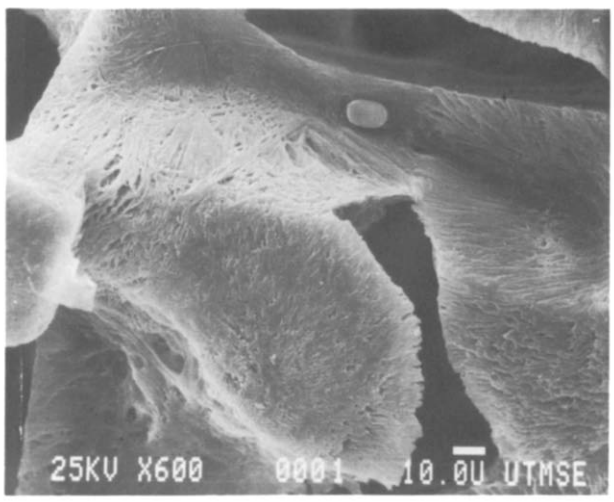

Figure 12 Spherulite deformation caused by HMB crystal occlusion; 30 wt% iPP crystallized at $\Delta T = 28$ K ($T_c = 403$ K)

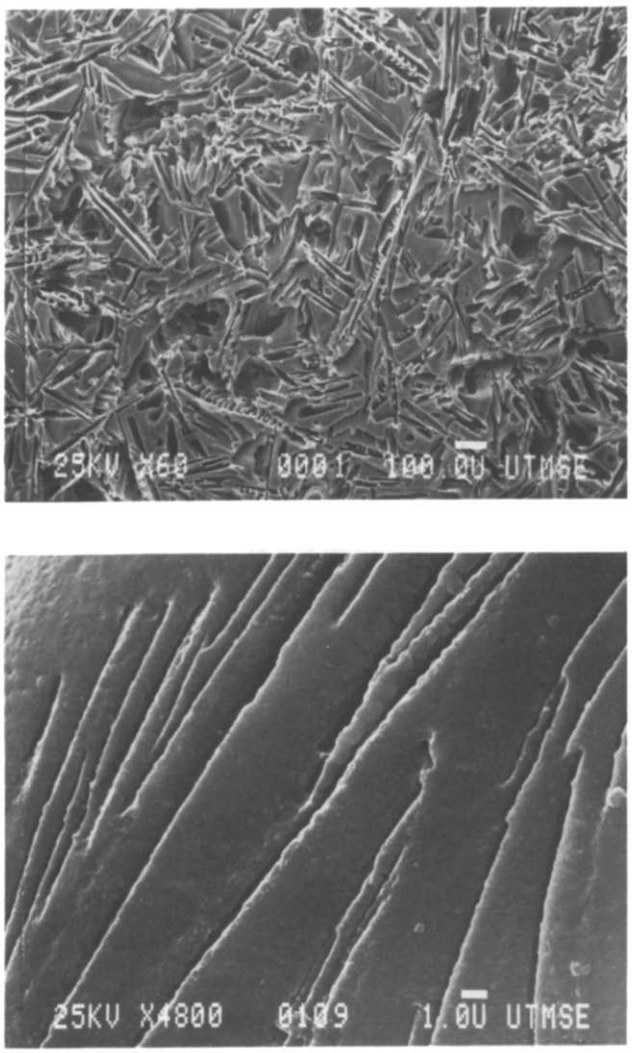

Figure 13 Primary and interspersed secondary needle-like pores; formed from 30 wt% iPP crystallized at $\Delta T = 56$ K ($T_c = 375$ K)

Spherulites were deformed near HMB crystals that had crystallized prior to the iPP crystallization for 30, 50 and to some extent 70 wt% iPP. The competition of phase separation events was shown to be instrumental in determining structure. A lack of discernible spherulite structure occurred in samples $W_p \leqslant 0.70$ and $\Delta T > 56$ K. This loss of spherulite structure is probably due to rapid crystallization of both components, with a resulting decrease in crystal size and a mutual disruption of structure. Spherulite size decreased at increased supercooling for all blends, in agreement with the increase in nucleation density that is expected as ΔT is increased.

The appearance of subtle morphological features such as cross-hatched, tangential lamellae was most clearly observed at low supercooling and low polymer concentrations.

ACKNOWLEDGEMENTS

The authors gratefully acknowledge the generous financial support of the Central Research Technology Development Laboratory of the 3M Company, St Paul, MN, and the Texas Advanced Technology Program.

REFERENCES

1 Hiatt, W. C., Vitzthum, G. H., Wagener, K. B., Gerlach, K. and Josefiak, C. in 'Materials Science of Synthetic Membranes' (Ed. D. R. Lloyd), ACS Symposium Series No. 269, American Chemical Society, Washington, DC, 1985
2 Caneba, G. T. and Soong, D. S. *Macromolecules* 1985, **18**, 2538
3 Caneba, G. T. and Soong, D. S. *Macromolecules* 1985, **18**, 2545
4 Lloyd, D. R., Kinzer, K. E. and Tseng, H. S. *J. Membr. Sci.* 1990, **52**, 239
5 Lloyd, D. R., Kim, S. S. and Kinzer, K. E. *J. Membr. Sci.* 1991, **64**, 1
6 Kim, S. S. and Lloyd, D. R. *J. Membr. Sci.* 1991, **64**, 13
7 Lim, G. B. A., Kim, S. S., Ye, Q., Wang, Y. F. and Lloyd, D. R. *J. Membr. Sci.* 1991, **64**, 31
8 Kim, S. S., Lim, G. B. A., Alwattari, A. A., Wang, Y. F. and Lloyd, D. R. *J. Membr. Sci.* 1991, **64**, 41
9 Alwattari, A. A. and Lloyd, D. R. *J. Membr. Sci.* 1991, **64**, 55
10 McGuire, K. S., Lloyd, D. R. and Lim, G. B. A. *J. Membr. Sci.* 1993, **79**, 27
11 Castro, A. J. US Patent 4247498, 1981
12 Vitzthum, G. H. and Davis, M. A. US Patent 4490431, 1984
13 Shipman, G. H. US Patent 4539256, 1985
14 Mrozinski, J. S. US Patent 4726989, 1988
15 Kinzer, K. E. US Patent 4867881, 1989
16 Lopatin, G., Yen, L. and Rogers, R. R. Eur. PAT. Appl. 88, 106209.5, 1988
17 Alwattari, A. and Lloyd, D. R. unpublished results
18 Lopez, J. M. R. and Gedde, U. W. *Polymer* 1988, **29**, 1037
19 Brana, M. T. C., Sainz, J. I. I., Terselius, B. and Gedde, U. W. *Polymer* 1989, **30**, 410
20 Norton, D. R. and Keller, A. *J. Mater. Sci.* 1984, **19**, 447
21 Norton, D. R. and Keller, A. *Polymer* 1985, **26**, 704
22 Keith, H. D. and Padden, F. J. *J. Appl. Phys.* 1964, **35**, 1270, 1286
23 Keith, H. D., Padden, F. J. and Russell, T. P. *Macromolecules* 1989, **22**, 666
24 Lotz, B. and Wittmann, J. C. *J. Polym. Sci., Polym. Phys. Edn.* 1986, **24**, 1541
25 Khoury, F. *J. Res. Natl. Bur. Stand. (A)* 1966, **70**, 29
26 Alwattari, A. PhD Thesis, University of Texas at Austin, 1990
27 Gezovich, D. M. and Geil, P. H. *Polym. Eng. Sci.* 1968, **8**, 202
28 Bassett, D. C. *CRC Crit. Rev. Solid State Mater. Sci.* 1983, **12**, 97
29 Temple Black, J. *Appl. Polym. Symp.* 1971, **16**, 105
30 Wang, Y. F. PhD Thesis, University of Texas at Austin, 1989
31 Olley, R. H., Hodge, A. M. and Bassett, J. J. *J. Polym. Sci. Polym. Phys. Edn.* 1979, **17**, 627
32 Naylor, K. L. and Phillips, P. J. *J. Polym. Sci., Polym. Phys. Edn.* 1983, **21**, 2011
33 Olley, R. H. and Bassett, D. C. *Polymer* 1982, **23**, 1707
34 Hodge, A. M., Kiss, G., Lotz, B. and Wittmann, J. C. *Polymer* 1982, **23**, 985
35 Kojima, M. and Satake, H. *J. Polym. Sci., Polym. Phys. Edn.* 1982, **20**, 2153
36 Thorpe, T. E. and Hambly, F. J. *J. Chem. Soc.* 1888, **53**, 175
37 Natta, G. and Corradini, P. *Nuovo Cim. Suppl.* 1960, **15**, 1
38 Keith, H. D., Padden, F. J. Walter, N. M. and Wycoff, M. W. *J. Appl. Phys.* 1959, **30**, 1485
39 Turner-Jones, A., Aizlewood, J. M. and Beckett, D. R. *Makromol. Chem.* 1964, **75**, 134
40 Bartczak, Z., Galeski, A. and Martuscelli, E. *Polym. Eng. Sci.* 1984, **9**, 1155